Available online at www.sciencedirect.com
SCIENCE DIRECT®
Journal of Organometallic Chemistry 688 (2003) 100–111
Journal of Organometallic Chemistry
www.elsevier.com/locate/jorganchem

Structural dynamics and ligand mobility in carboxylate and dithiocarbamate complexes of Ru(II) containing 1,1′-bis(diphenylphosphino)ferrocene (dppf)

Xiu Lian Lu, Sin Yee Ng, Jagadese J. Vittal, Geok Kheng Tan, Lai Yoong Goh *, T.S. Andy Hor *

Department of Chemistry, National University of Singapore, Kent Ridge, Singapore 119260, Singapore

Received 11 June 2003; received in revised form 29 August 2003; accepted 29 August 2003

Abstract

Ruthenium(II) carboxylate and dithiocarbamate complexes containing 1,1′-bis(diphenylphosphino)ferrocene (dppf) were synthesized by displacement of triphenylphosphine in $Ru(RCOO)_2(PPh_3)_2$ (R = Me, Et, Ph) and $Ru(SC(S)NEt_2)_2(PPh_3)_2$ with dppf. The complexes $Ru(RCOO)_2$(dppf) (**1a**: R = Me, **1b**: R = Et, **1c**: R = Ph) and $Ru(SC(S)NEt_2)_2$(dppf) (**3**) were obtained in yields of 78–93%. The crystal structures of these complexes show coordination of the phosphorus atoms of dppf and four oxygen/sulphur atoms of carboxylate/dithiocarbamate ligands to a Ru(II) centre with axial-bond-distorted octahedral geometry. Two pseudo-polymorphic forms of **1c** were isolated and crystallographically characterized. VT-^{1}H- and $^{31}P\{^1H\}$-NMR spectral studies of **1a**–**c** and **3** demonstrate mono- and bidentate exchange behaviour of the carboxylate or dithiocarbamate ligands, together with concerted twisting of the Cp rings of the dppf ligand. Complex **1c** in CH_3CN at room temperature gives $Ru(PhCOO)_2$(dppf)$(CH_3CN)(H_2O)$ (**2**), the crystal structure of which reveals two monodentate benzoate ligands around octahedral ruthenium and intramolecular inter-ligand H-bonding interaction between the coordinated H_2O and the pendant carboxylate oxygen atoms. The interrelationship of crystallographic properties, structural dynamics, ligand mobility and chemical instability of these complexes will be described.

Keywords: Ruthenium; Carboxylate; Dithiocarbamate; 1,1′-Bis(diphenylphosphino)ferrocene (dppf); Structural dynamics

1. Introduction

Ruthenium carboxylate phosphine complexes have attracted much attention because of their structural diversity [1–6], extensive chemistry [4–8] and catalytic applications [9–15]. In particular, many ruthenium carboxylate complexes containing diphosphines are efficient catalysts [12–16]. Such carboxylate diphosphine complexes are easily synthesized by substitution of PPh_3 in $Ru(RCO_2)_2(PPh_3)_2$. However, the reaction of $Ru(RCO_2)_2(PPh_3)_2$ with metallocene-based diphosphine ligands, such as 1,1′-bis(diphenylphosphino)ferrocene (dppf) has not been studied. In view of the growing awareness that dppf enhances the catalytic activity of metal complexes [7–19], this will be of interest and in this paper, we describe the structures and dynamic behaviour of some of these dppf ruthenium complexes with carboxylate or dithiocarbamate as coligand.

2. Experimental

All reactions were performed under dry nitrogen using Schlenk techniques. Solvents were freshly distilled from standard drying agents. ^{1}H- and $^{31}P\{^1H\}$-NMR spectra were recorded on a Bruker ACF300 FT NMR spectrometer, with chemical shifts referenced to residual non-deuterio solvent and external H_3PO_4, respectively. The VT-^{1}H-NMR spectra of complex **3** was recorded on a Bruker ACF500 FT NMR spectrometer. IR spectra were measured in KBr pellet on a Perkin–Elmer 1600

* Corresponding authors. Tel.: +65-6874-2677; fax: +65-6779-1691.
E-mail addresses: chmgohly@nus.edu.sg (L.Y. Goh), andyhor@nus.edu.sg (T.S.A. Hor).

0022-328X/03/$ - see front matter © 2003 Elsevier B.V. All rights reserved.
doi:10.1016/j.jorganchem.2003.08.037

spectrometer. FAB mass spectra were obtained on a Finnigan MAT95XL-T spectrometer. All elemental analyses were carried out in-house. $RuCl_2(PPh_3)_3$ [20], $Ru(RCOO)_2(PPh_3)_2$ (R = Me, Et, Ph) [9,21], and $Ru[SC(S)N(CH_3CH_2)_2]_2(PPh_3)_2$ [22] were synthesized according to published procedures. Other reagents used were of AR grade obtained from commercial sources.

2.1. Synthesis

2.1.1. *Ru(RCOO)$_2$(dppf) (**1a**: R = Me; **1b**: R = Et; **1c**, R = Ph)*

A yellow solution of $Ru(MeCOO)_2(PPh_3)_2$ (50 mg, 0.067 mmol) and dppf (37 mg, 0.069 mmol) in CH_2Cl_2 (5 ml) was stirred for ca. 1 h at room temperature (r.t.). The yellow product solution was concentrated to ca. 1 ml and hexane (ca. 3 ml) was added. Yellow crystals of $Ru(MeCOO)_2$(dppf) (**1a**) were obtained after cooling at −5 °C for ca. 4 h (42 mg, 0.054 mmol, 80% yield). Anal. Calc. for $RuFeC_{38}H_{34}O_4P_2$: C, 59.0; H, 4.4; P, 8.0; Fe, 7.2. Found: C, 58.8; H, 4.5; P, 7.8; Fe, 6.8%. ^{1}H-NMR (δ, $CDCl_3$, 300 K): 1.38 (s, 6H, CH_3), 4.25 (s, 8H, C_5H_4), 7.34 and 7.37 (br., overlapping singlets, 12H, C_6H_5) together with 7.58 (s, $\nu_{1/2}$ = 29 Hz, 8H, C_6H_5). ^{31}P-NMR (δ, $CDCl_3$): 62.3 (s, dppf). FAB$^+$-MS: *m/z* 774 $[M+H]^+$, 714 $[M-CH_3COO+H]^+$, 655 $[M-2(CH_3COO)+H]^+$. IR (KBr, cm^{-1}), ν(OCO(biden-bidentate)): 1459(s), 1434(m, sh).

A similar reaction of $Ru(EtCOO)_2(PPh_3)_2$ (50 mg, 0.065 mmol) with dppf (36 mg, 0.065 mmol) gave $Ru(EtCOO)_2$(dppf) (**1b**) as red crystals (41 mg, 0.051 mmol, 78% yield). Anal. Calc. for $RuFeC_{38}H_{38}O_4P_2$: C, 59.9; H, 4.7; P, 7.7. Found: C, 59.8; H, 4.7; P, 8.1%. ^{1}H-NMR (δ, $CDCl_3$, 300 K): 0.67 (t, *J* = 8 Hz, 6H, CH_3), 1.70 (q, *J* = 8 Hz, 4H, CH_2), 4.24 (s, 4H, C_5H_4), 4.30 (s, broad, 4H, C_5H_4), 7.32–7.38 (*pseudo*-quartet with main peaks centred at δ 7.35 and 7.32, 12H, C_6H_5P), 7.57 (s, $\nu_{1/2}$ = 21 Hz, 8H, C_6H_5P). ^{31}P-NMR (δ, $CDCl_3$): 62.5 (s, dppf). FAB$^+$-MS: *m/z* 802 $[M+H]^+$, 729 $[M-CH_3CH_2COO+H]^+$, 655 $[M-2CH_3CH_2COO+H]^+$. IR (KBr, cm^{-1}), ν(OCO(bidentate)): 1504(m), 1471(s),1439(vs); ν(CH): 3057(w).

A yellow solution of $Ru(PhCOO)_2(PPh_3)_2$ (50 mg, 0.056 mmol) with dppf (32 mg, 0.057 mmol) in CH_2Cl_2 (5 ml) was stirred for ca. 1 h at r.t. The yellow product solution was concentrated to ca. 1 ml and hexane (ca. 3 ml) was added. After cooling at 0 °C for ca. 4 h, red crystals of $Ru(PhCOO)_2$(dppf) (**1c**) (ca. 45 mg, 0.050 mmol, 88% yield) and yellow crystals of **1c**·*n*H_2O (ca. 3 mg, 0.003 mmol, 5% yield) were found to have formed on different parts of the walls of the flask. Both types were yellow when pulverized, and possessed indistinguishable IR, NMR and MS-FAB spectra. Anal. Calc. for $RuFeC_{48}H_{38}O_4P_2$: C, 64.2; H, 4.2; P, 6.9; Fe, 6.2. Found for **1c**: C, 63.9; H, 4.2; P, 5.9; Fe, 5.9%. ^{1}H-NMR (δ, $CDCl_3$, 300 K): 4.27 (s, 4H, β-H's on C_5H_4), 4.41 (s, 4H, α-H's on C_5H_4), 7.16 and 7.31 (each triplet, *J* = 8 Hz, 6H, C_6H_5COO) sitting on two overlapping broad peaks centred at δ 7.17 and 7.25 ($\nu_{1/2}$ 32 and 24 Hz, respectively, 8H, C_6H_5P), 7.57 (d, *J* = 8 Hz, 4H, C_6H_5COO) sitting on a broad peak centred at δ 7.61 ($\nu_{1/2}$ 30 Hz, 12H, C_6H_5P). ^{31}P-NMR (δ, $CDCl_3$): 62.6 (s, dppf). FAB$^+$-MS: *m/z* 777 $[M-PhCOO+H]^+$, 655 $[M-2PhCOO+H]^+$. IR (KBr, cm^{-1}), ν(OCO (bidentate)): 1499(m), 1422(s).

Because it appeared that more yellow crystals were obtained during a longer recrystallization time at low temperature, the above reaction was repeated both in refluxing toluene and in CH_2Cl_2 at 5 °C; these conditions gave mainly red and yellow crystals, respectively. X-ray diffraction quality red crystals of **1c** were obtained from the high-temperature reaction by recrystallization of the product in 1:3 CH_2Cl_2–hexane (layering) at r.t. after overnight standing. From the yellow microcrystalline product of the low-temperature reaction were obtained diffraction-quality reddish yellow crystals of **1c**·1.25H_2O from 1:2 CH_2Cl_2–hexane (layering) after 8 h at −5 °C.

2.1.2. *Ru(PhCOO)$_2$(dppf)(CH_3CN)(H_2O) (**2**)*

CH_3CN (8 ml) was added to $Ru(PhCOO)_2$(dppf) (**1c**) (100mg, 0.11 mmol), and the suspension was stirred for 3 h at r.t. The clear yellow solution was concentrated to ca. 2 ml and ether (ca. 8 ml) was added. Yellow crystals of $Ru(PhCOO)_2$(dppf)(CH_3CN)(H_2O) (**2**) were obtained after cooling at 0 °C for 4 h followed by standing at r.t. for 12 h (83 mg, 0.087 mmol, 77% yield). Anal. Calc. for $RuFeC_{50}H_{43}NO_5P_2$: C, 62.7; H, 4.5; N, 1.5. Found: C, 62.7; H, 4.7; N, 1.4%. ^{1}H-NMR (δ, $CDCl_3$, 300 K) shows two species, possibly isomers, which vary with concentration. Major isomer: 1.81 (s, 3H, CH_3CN), 4.23 (s, 3H, C_5H_5), 4.30 (s, 3H, C_5H_5), 4.62 (broad s, 2H, C_5H_5), 7.05–7.75 (m, 30H, C_6H_5COO and C_6H_5P); Minor isomer: 1.87 (s, 3H, CH_3CN), 3.47 (s, 1H, C_5H_5), 3.85 (s, 1H, C_5H_5), 4.07 (s, 2H, C_5H_5), 4.53 (s, 3H, C_5H_5), 5.46 (s, 1H, C_5H_5), 7.05–8.43 (m, 30H, C_6H_5COO and C_6H_5P); ^{31}P-NMR (δ, $CDCl_3$): 54.7 (d, *J* = 34 Hz), 60.3 (d, *J* = 34 Hz). FAB$^+$-MS: *m/z* 898 $[M-CH_3CN-H_2O+H]^+$, 818 $[M-PhCOO-H_2O+H]^+$, 777 $[M-PhCOO-CH_3CN-H_2O+H]^+$, 655 $[M-2PhCOO-CH_3CN-H_2O+H]^+$. IR (KBr, cm^{-1}), ν(CH_3CN): 2277(s). ν(OCO (monodentate)): 1624(m), 1380(s).

2.1.3. *Ru[SCSNEt$_2$]$_2$(dppf) (**3**)*

A yellow solution of $Ru(SC(S)NEt_2)_2(PPh_3)_2$ (50 mg, 0.054 mmol) and dppf (30 mg, 0.054 mmol) in toluene (5 ml) was refluxed for ca. 2 h. The solution was concentrated to ca. 0.2 ml and CH_2Cl_2 (ca. 1 ml) was added to redissolve some precipitated solids. Hexane (ca. 3 ml) was added and orange–yellow crystals of

$Ru(SCSNEt_2)_2(dppf)$ (**3**) were obtained after cooling overnight at −5 °C (41 mg, 0.043 mmol, 80% yield). Anal. Calc. for $RuFeC_{44}H_{48}N_2P_2S_2$: C, 55.5; H, 5.1; N, 2.9. Found: C, 55.7; H, 5.4; N, 2.6%. ^{1}H-NMR (δ, $CDCl_3$, 300 K): 0.98 (s, br., 12H, CH_3), 3.24 (s, $v_{1/2} = 42$ Hz, 2H, CH_2), 3.53 (s, $v_{1/2} = 33$ Hz, 6H, CH_2), 4.20 (s, 2H, C_5H_4), 4.36 (s, 2H, C_5H_4), 4.44 (s, 4H, C_5H_4), 7.17 and 7.24 (overlapping triplets, $J = 8$ Hz, 12 H, C_6H_5P), 7.68 (s, $v_{1/2} = 26$ Hz, 8H, C_6H_5P). ^{31}P-NMR (δ, $CDCl_3$): 48.9 (s, dppf). FAB$^+$-MS: m/z 952 $[M+H]^+$, 804 $[M-SC(S)NEt_2+H]^+$. IR (KBr, cm^{-1}): ν(SC(S)): 1485(m), 1428(m), 1271(s).

2.2. X-ray diffraction analysis

Diffraction-quality single crystals of **1c** and **1c**·$1.25H_2O$ were obtained as described above; those of **1a**–**b** and **3**·$2CH_2Cl_2$·$2H_2O$ were also obtained from CH_2Cl_2 layered with hexane, after 4–8 h at −5 °C, while single crystals of **2**·CH_3CN·$0.5H_2O$ were obtained from CH_3CN layered with ether after 4 h at 0 °C followed by 12 h at r.t. The crystals were mounted on quartz fibres. X-ray data were collected on a Bruker AXS SMART CCD diffractometer, using Mo–K_α radiation ($\lambda = 0.71073$ Å) at 223 K except for **1a** at 296 K.

The program SMART [23] was used for collecting the intensity data, and for the determination of lattice parameters, SAINT [23] was used for integration of the intensity of reflections and scaling, SADABS [24] was used for absorption correction and SHELXTL [25] for space group and structure determination, least-squares refinements on F^2. The structure was solved by direct methods to locate the heavy atoms, followed by difference maps for the light, non-hydrogen atoms. The Cp and Ph hydrogens were placed in calculated positions. There are 2.5 disordered water molecules in nine places in the yellow crystal of **1c**, and two H_2O and two CH_2Cl_2 solvents per formula unit in **3**. Crystal data and refinement parameters are given in Table 1.

3. Results and discussion

3.1. Reactions

The ruthenium carboxylate dppf complexes were synthesized in high yields by substitution of PPh_3 in $Ru(RCOO)_2(PPh_3)$ (**1a**: R = Me, **1b**: R = Et, **1c**: R = Ph) at ambient temperature as shown in Scheme 1. For R = Ph, the reaction produced a mixture of red crystals of **1c**, as major product and a small amount of yellow crystals of solvate, **1c**·nH_2O; both forms were yellow when pulverized and were indistinguishable in their IR, NMR and MS spectra. It was observed that the red form was the main product from a high-temperature reaction, and recrystallized as red single crystals of **1c** from CH_2Cl_2–hexane at room temperature, whereas the yellow form was the major product from a low-temperature reaction and recrystallized as reddish yellow single crystals of **1c**·$1.25H_2O$ after 8 h at −5 °C in CH_2Cl_2–hexane. The difference between them shows up in their structures which reveal 2.5 disordered water molecules in the asymmetric unit of the hydrate.

Complexes **1a**–**c** are stable in the solid state; in CH_2Cl_2, all are very stable, but in $CDCl_3$, **1b** is very unstable, followed by **1a** and **1c**.

The ruthenium dithiocarbamate dppf complex **3** was prepared via an analogous reaction of $Ru(SC(S)NEt_2)_2(PPh_3)_2$ with dppf for 2 h in refluxing toluene (Scheme 2). Unlike complexes **1a**–**c**, this compound was found to be very stable in both $CDCl_3$ and CH_2Cl_2. $Ru(PhCOO)_2$(dppf) (**1c**/**1c**·nH_2O) in CH_3CN gives $Ru(PhCOO)_2(CH_3CN)(H_2O)$(dppf) (**2**) in high yield after stirring for 3 h at ambient temperature.

3.2. Structures

It is of interest to examine the structure of these tris-chelate complexes, since the chelating behaviour of a large-bite ligand such as dppf and a small-bite ligand such as carboxylate and dithiocarbamate is expected to be significantly different. We also wish to seek an understanding of the unexpected high instability of **1** in solution and a structural explanation for the easy conversion of **1c** to **2** in CH_3CN.

A detailed crystallographic analysis of the key complexes showed that crystals of **1a**, **1b**, **1c**·$1.25H_2O$ and **2**·CH_3CN·$0.5H_2O$ are triclinic, possessing $P\bar{1}$ space group, while those of **1c** and **3**·$2CH_2Cl_2$·$2H_2O$ are monoclinic with space groups Cc and $C2/c$, respectively.

Complexes **1a**–**c** and **3** are isostructural (Figs. 1–4), with three chelates (dppf and two bidentate carboxylate or dithiocarbamate ligands) at 18e-Ru centres. Since the bite angle of the diphosphine (P–Ru–P: 95.48(4)–100.64(9)°) is significantly larger than the chelate angle of the dithiocarbamate (S–Ru–S: 71.94(6)°) or the carboxylate (O–Ru–O: 59.3(3)–61.76(12)°), a regular octahedral structure cannot be achieved, giving rise to distortion in the axial bonds. The structures of **1c** and **1c**·$1.25H_2O$ are pseudo-polymorphic. There are two independent molecules in the asymmetric unit in **1c** and **1c**·$1.25H_2O$.

The structure of **2** (Fig. 5) shows two monodentate benzoate ligands at an 18e-Ru centre. This is the only structure among the complexes here that can be suitably described as (near)octahedral, made possible by removing the geometric demands of the small bite angles of chelating carboxylate ligands. The two monodentate carboxylates are *trans* to different ligands (phosphine and CH_3CN), and the two phosphine donors are *trans* to different donors (aqua and carboxylate). There exists

Table 1
Crystal data and parameters related to the structure determination and refinement for complexes

Complexes	**1a**	**1b**	**1c**	**1c**·1.25H_2O	**2**·CH_3CN·0.5H_2O	**3**·2CH_2Cl_2·2H_2O
Empirical formula	$C_{38}H_{34}FeO_4P_2Ru$	$C_{40}H_{38}FeO_4P_2Ru$	$C_{48}H_{38}FeO_4P_2Ru$	$C_{48}H_{40.50}FeO_{5.25}P_2Ru$	$C_{52}H_{47}FeN_2O_{5.50}P_2Ru$	$C_{46}H_{56}Cl_4FeN_2O_2P_2Ru$
Formula weight	773.51	801.56	897.64	920.16	1006.7	1157.83
Temperature (K)	296(2)	223(2)	223(2)	223(2)	223(2)	223(2)
Crystal system	Triclinic	Triclinic	Monoclinic	Triclinic	Triclinic	Monoclinic
Space group	$P\bar{1}$	$P\bar{1}$	Cc	$P\bar{1}$	$P\bar{1}$	$C2/c$
a (Å)	9.4134(5)	9.2367(6)	10.3305(3)	10.3963(4)	10.6184(7)	29.119(3)
b (Å)	10.1319(6)	13.5453(8)	17.9596(5)	19.2080(8)	14.1725(9)	13.3221(12)
c (Å)	18.6193(11)	14.5017(9)	42.5516(12)	21.3477(9)	17.3114(11)	14.6545(12)
α (°)	96.112(1)	90.269(1)	90	87.271(1)	91.105(2)	90
β (°)	103.675(1)	100.939(1)	93.455(1)	81.658(1)	104.7390(10)	112.731(2)
γ (°)	100.951(1)	93.342(1)	90	82.205(1)	108.8170(10)	90
V (Å^3)	1672.60(17)	1778.14(19)	7880.3(4)	4177.2(3)	2370.1(3)	5243.3(8)
Z	4	2	8	4	2	4
D_{calc} (g cm^{-3})	1.536	1.497	1.513	1.463	1.411	1.467
Absorption coefficient (mm^{-1})	0.833	0.963	0.879	0.833	0.742	1.027
F(000)	1882	820	3664	1882	1034	2376
Crystal size (mm)	0.24 × 0.16 × 0.12	0.38 × 0.28 × 0.04	0.24 × 0.18 × 0.10	0.24 × 0.16 × 0.12	0.38 × 0.30 × 0.30	0.46 × 0.36 × 0.12
Theta range for data collection (°)	1.46–25.00	1.43–30.08	0.96–25.00	1.46–25.00	1.22–25.00	1.52–25.00
Index ranges	$-12 \le h \le 12$, $-22 \le k \le 22$, $-25 \le l \le 25$	$-10 \le h \le 12$, $-19 \le k \le 19$, $-20 \le l \le 16$	$-12 \le h \le 12$, $-21 \le k \le 17$, $-50 \le l \le 44$	$-12 \le h \le 12$, $-22 \le k \le 22$, $-25 \le l \le 25$	$-12 \le h \le 12$, $-16 \le k \le 14$, $-20 \le l \le 20$	$-34 \le h \le 31$, $-15 \le k \le 15$, $-17 \le l \le 16$
Reflections collected	45 416	14 398	22 723	45 416	13 594	14 699
Independent reflections	14 731	9713	11 428	14 731	8293	4617
Max/min transmission	0.9170, 0.8017	0.9625, 0.7110	0.9123, 0.6830	0.9170, 0.8017	1.0000, 0.6123	0.8330, 0.5223
Data/restraints/parameters	14731/0/11045	9713/0/428	11428/2/481	14731/0/1045	8293/10/512	4617/1/1264
Goodness-of-fit on F^2 [c]	1.039	1.121	1.145	1.039	1.080	1.182
Final R indices $[I > 2\sigma(I)]$ [a,b]	$R_1 = 0.0424$, $wR_2 = 0.1066$	$R_1 = 0.0463$, $wR_2 = 0.1070$	$R_1 = 0.0639$, $wR_2 = 0.1317$	$R_1 = 0.0424$, $wR_2 = 0.1066$	$R_1 = 0.0629$, $wR_2 = 0.1659$	$R_1 = 0.0846$, $wR_2 = 0.2551$
R indices (all data)	$R_1 = 0.0618$, $wR_2 = 0.1116$	$R_1 = 0.0532$, $wR_2 = 0.1169$	$R_1 = 0.0925$, $wR_2 = 0.1826$	$R_1 = 0.0618$, $wR_2 = 0.1116$	$R_1 = 0.0689$, $wR_2 = 0.1727$	$R_1 = 0.0978$, $wR_2 = 0.2716$
Largest difference peak and hole (e Å^{-3})	0.958 and −0.434	1.697 and −0.802	1.265 and −0.563	0.958 and −0.434	1.685 and −1.133	2.857 and −0.786

[a] $R = (\Sigma|F_o| - |F_c|)\Sigma|F_o|$.
[b] $R_w = [(\Sigma\omega|F_o| - |F_c|)^2/\Sigma\omega|F_o|^2]^{1/2}$.
[c] $GoF = [(\Sigma\omega|F_o| - |F_c|)^2/(N_{obs} - N_{param})]$.

inter-ligand hydrogen-bonding between the aqua protons and the two pendant carboxylate oxygen atoms of monodentate benzoates. This intramolecular interaction stabilizes the molecule by decreasing the lability of unibidentate exchange (discussed below). Indeed, it was observed that unlike **1a**–**c**, **2** no longer decomposed in $CDCl_3$, indicative of the arrest of exchange behaviour. The IR spectrum in KBr pellet shows coordinated CH_3CN at ν 2277 cm^{-1}. This compares well with values of 2270 and 2310 cm^{-1} for reported cases of CH_3CN coordinated to Ru [26]. The IR data also support the presence of unidentate carboxylate ligands [27]. It is noted that the asymmetric arrangement of the ligands in **2** resulted in an unusual chiral Ru(II) phosphine carboxylate complex, which possibly has a potential in asymmetric catalysis.

Selected bond lengths and bond angles of the complexes are collectively given in Table 2. The Ru–O bond lengths gradually decrease in the order: **1a** > **1b** > **1c**, in agreement with the order of nucleophilicity of the carboxylate groups (PhCOO > EtCOO > MeCOO), indicating that the higher steric demands of PhCOO has not offset electronic effects on the magnitude of the Ru–O bond length. The bond distances of Ru to O, "*trans*" to phosphorus atoms, are considerably longer than that "*trans*" to oxygen atoms. This is due to the high *trans* effect of the strongly σ-donating phosphorus atom. The difference in the two Ru to O bond distances is most

$$RuCl_2(PPh_3)_3 + Na(O_2CR) \longrightarrow Ru(O_2CR)_2(PPh_3)_2 \xrightarrow{dppf} Ru(O_2CR)_2(dppf)$$

1a: R = CH_3
1b: R = CH_2CH_3
1c: R = Ph

Scheme 1.

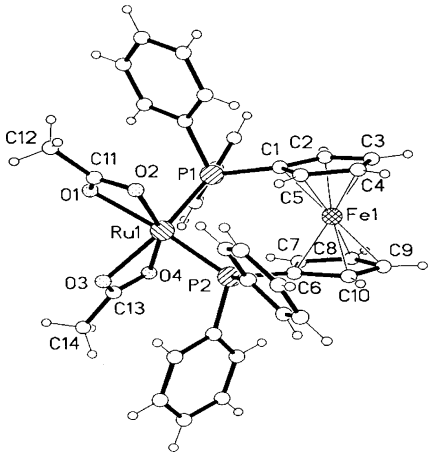

Fig. 1. Molecular structure of $Ru(CH_3COO)_2(dppf)$ (**1a**).

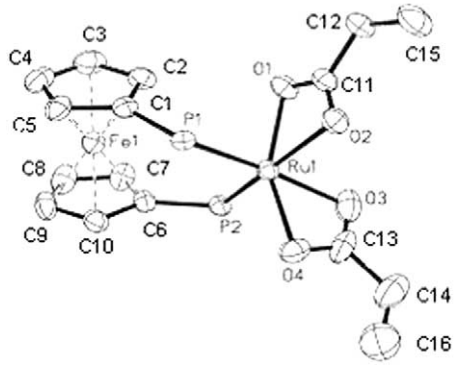

Fig. 2. ORTEP diagram of $Ru(EtCOO)_2(dppf)$ (**1b**). Hydrogen atoms are omitted. Thermal ellipsoids are drawn to 50% probability level.

evident in **1c** and **1c**·1.25H_2O. Similar observations are found in **2**. The Ru–P distance (2.3174(18) Å) in **3** is significantly longer than the corresponding Ru–P distance (2.2235(12)–2.2860(13) Å) in **1a**–**c**, whereas the difference between Ru–S (2.4175(18) Å) in **3** and Ru–O bond lengths in **1a**–**c** (2.108(3)–2.267(10) Å) is only reflective of the relative size of the sulphur and oxygen atoms. The C–S bond lengths in **3** (1.718(7) and 1.715(7) Å), slightly longer than the C=S double bond, are comparable to previously reported values for dithiocarbamate ligands (1.700(7)–1.79(2) Å) and the C–N distances (1.329(9)–1.467(9) Å), slightly longer than previous values (1.288(8)–1.52(9) Å) for dithiocarbamate complexes [28] are indicative of partial double-bond character (C–S, 1.81; C=S, 1.61; C–N, 1.47 and C=N, 1.27 Å) [29]. In accordance with the HSAB principle, the S-donor ligands of **3** bond more strongly to Ru than do the O-donor atoms of carboxylate ligands; this is reflected in the relative instability of complexes **1**.

In **1a**, the atoms in each acetate group are coplanar and the inter-planar angle is 106.4°. The structure of **1b** shows one CH_3 group pointing to the Ru centre (C11–C12–C15 = 114.3(3)°), whereas the other group points away from Ru (C13–C14–C16 = 113.5(5)°). The P–Ru–P bond angles of **1** decrease in the order: **1a** (99.58(5)°) > **1b** (97.95(3)°) > **1c** (96.53(13), 95.48(4)°), in accordance with the increasing steric demands of the R group in the carboxylate ligands.

3.3. NMR spectral studies

The ambient temperature proton NMR spectra show broad signals for the Cp protons (**1a**–**c**) or the ethyl protons (**1b**, **3**), suggesting that they are fluxional in solution. Fluxionality arising from uni-bidentate exchange processes of the carboxylate ligands would involve the interconversions of 14e↔16e↔18e Ru(II), which could have a catalytic implication. We therefore decided to study their variable-temperature (VT) NMR spectra in detail.

The VT proton resonances of the phenyl and Cp rings of $Ru(RCOO)_2(dppf)$ (**1a** and **1b**) in the range of 328–213 K in $CDCl_3$ are very similar. As shown for **1a** in Fig. 6(a), the Cp protons are observed as two overlapping singlets of approximately equal intensity at δ 4.29 and 4.24 at 328–313 K; the former peak broadens rapidly with lowering of temperature while the latter peak remains sharp to 258 K (δ 4.26), at which temperature line-broadening has set in; at 213 K and below complete resolution had occurred, giving four sharp signals at δ 4.41, 4.28, 4.23 and 4.11. This pattern of VT ^{1}H-NMR spectral variations is typical of the general fluxional behaviour of dppf complexes and has been attributed to

$$RuCl_2(PPh_3)_3 + NaSC(S)NEt_2 \longrightarrow Ru(S_2CNEt_2)_2(PPh_3)_2 \xrightarrow{dppf} Ru(S_2CNEt_2)_2(dppf)$$

3

Scheme 2.

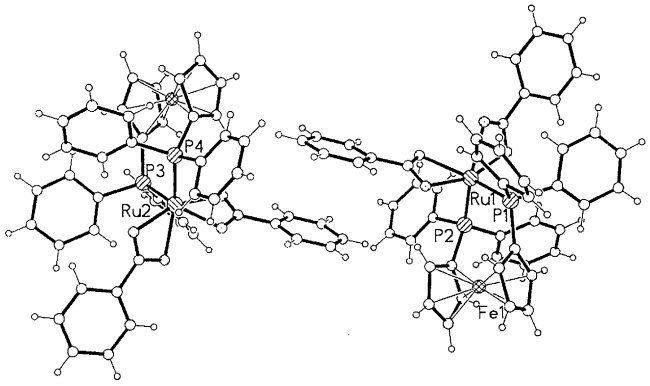

Fig. 3. Two independent molecules of $Ru(PhCOO)_2(dppf)$ (**1c**).

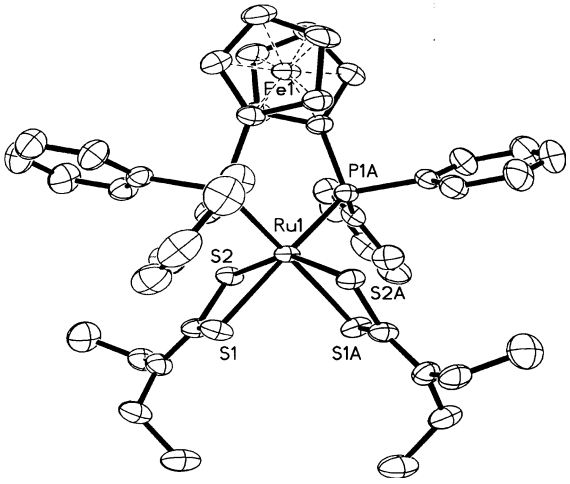

Fig. 4. ORTEP diagram of $Ru[SCSNEt_2]_2(dppf)$ (**3**). Hydrogen atoms are omitted. Thermal ellipsoids are drawn to 50% probability level.

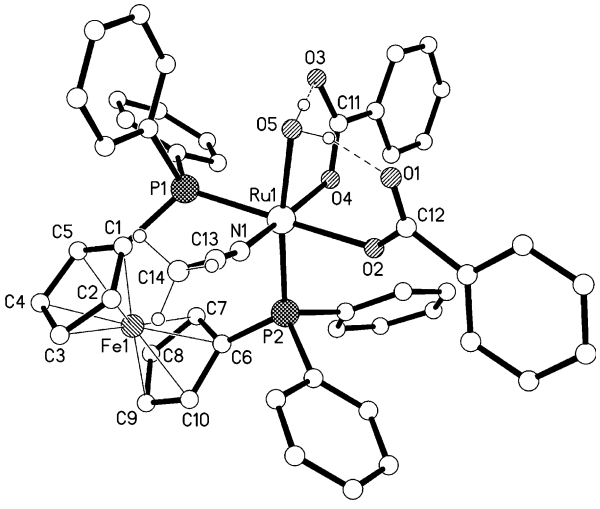

Fig. 5. Molecular structure of $Ru(PhCOO)_2(CH_3CN)(H_2O)dppf$ (**2**). Hydrogen atoms are omitted.

mutual twisting of the Cp rings and bridge-reversal at the metal [17]. In the temperature range studied, the only change seen in the Ph proton resonances is a slight shifting of the broad peak at δ 7.59 ($\nu_{1/2} = 18$ Hz) and multiplets at δ 7.31–7.38 at 328 K to lower field, being found at δ 7.68 ($\nu_{1/2} = 18$ Hz) together with two sets of overlapping multiples at δ 7.41–7.52 and 7.27–7.35 at 213 K. Throughout this temperature range, the singlet ^{31}P resonance remained unchanged (**1a**, δ 62.3; **1b**, δ 62.5). The Me resonance of the acetate groups in **1a** remained unchanged at δ 1.37, suggesting non-fluxional behaviour. This is in contrast to uni-bidentate fluxionality of acetate ligands, observed by Jia for $Ru(Cl)(OAc)(Cyttp)$ (ttp = $PhP(CH_2CH_2CH_2PPh_2)_2$) [3] and by Wong for $Ru(OAc)_2PPh_3(dppm)$ (dppm = $Ph_2P(CH_2)PPh_2$) [5] and also for the carboxylate ligands found in **1b**. The VT behaviour of the ethyl protons of **1b** is shown in Fig. 6(b). At 300 K, the Me protons are seen as one triplet at δ 0.70 and the CH_2 protons as a quartet at δ 1.70. As the temperature is lowered, these peaks broaden. At 243 K, the broad methylene peak has begun to resolve into two broad signals which at 213 K are seen at unresolved quartets as δ 1.46 ($J = 8$ Hz) and 1.89 ($J = 8$ Hz), while the Me resonance is still seen as one (unresolved triplet-like) signal. These VT features of the ethyl protons can be rationalized on the basis of bidentate–monodentate exchange of the carboxylate ligands, as shown in Fig. 7. At ambient temperature this process is fast, rendering equivalent the methylene protons and likewise the methyl protons. Below 233 K, the presence of two CH_2 signals suggests two inequivalent ethyl groups, pertaining to a mono- and a bidentate carboxylate ligand, respectively, as in species B′, which is likely to achieve six-coordination involving ligated solvent as shown in B. A similar mechanism has been proposed for rapid intramolecular exchange of mono- and bidentate carboxylate ligands in $Ru(OAc)_2(PPh_3)$(diphosphine) (diphosphine = dppm, dppb, dppp) [1]. It is not immediately obvious why these processes have so little effect on the chemical environments of the P atoms of the dppf ligand. One possibility is that the predominant intermediate species is indeed the five-coordinate species B′, which being stereochemically non-rigid, renders the P atoms non-differentiating in the NMR time-scale.

The VT-proton and $^{31}P\{^1H\}$-NMR spectra of $Ru(PhCOO)_2(dppf)$ (**1c**) in the range 328–213 K in $CDCl_3$ are shown in Fig. 8. In the temperature range 328–258 K the Cp protons are observed as singlets at δ 4.42 and 4.28, with the former peak rapidly increasing in linewidth as the temperature is lowered, from $\nu_{1/2}$ of 7 Hz at 328 K to 69 Hz at 258 K. In this temperature range, there is little change in the Ph proton resonances which at 300 K appear as a set of multiplets consisting of a triplet at δ 7.17 ($J = 8$ Hz) on a broader peak ($\nu_{1/2} = 32$ Hz), overlapping with another broad peak centred at δ 7.25 ($\nu_{1/2} = 24$ Hz), together with a doublet at δ 7.57 ($J = 8$ Hz) on top of a broad base centred at δ 7.61 ($\nu_{1/2} = 30$ Hz). In contrast to a single temperature-

Table 2
Selected bond lengths (Å) and angles (°)

	1a	**1b**	**1c**	**1c**·1.25H_2O	**2**·CH_3CN·0.5H_2O	**3**·2CH_2Cl_2·2H_2O
	Ru(CH_3COO)$_2$dppf	Ru(CH_3CH_2COO)$_2$dppf	Ru(PhCOO)$_2$dppf	Ru(PhCOO)$_2$dppf	Ru(PhCOO)$_2$(CH_3CN)(H_2O)dppf	Ru[$S_2CN(CH_3CH_2)_2$]$_2$dppf
Bond lengths						
Ru1–P1	2.2741(14)	2.2602(8)	2.236(3)	2.2235(12)	2.2633(10)	2.3174(18)
Ru1–P2	2.2860(13)	2.2719(8)	2.224(4)	2.2512(12)	2.3004(12)	2.3174(18)
Ru1–X1	2.178(3)	2.143(2)	2.110(9)	2.127(3)	Ru1–O2 2.150(3)	2.4175(18)
Ru1–X2	2.129(3)	2.184(2)	2.267(10)	2.190(3)	Ru1–O4 2.100(3)	2.4109(16)
Ru1–X3	2.139(3)	2.180(3)	2.240(9)	2.207(3)	Ru1–O5 2.157(3)	
Ru1–X4	2.118(3)	2.118(2)	2.109(8)	2.108(3)		
O1–C11	1.255(6)	1.284(4)	1.272(15)	1.273(5)	C(11)–O(3) 1.248(6)	
O2–C11	1.259(5)	1.265(4)	1.221(17)	1.264(5)	C(11)–O(4) 1.264(6)	
O3–C13	1.258(6)	1.253(6)	1.232(15)	1.259(5)	C(12)–O(1) 1.238(5)	
O4–C13	1.263(6)	1.3056(5)	1.248(15)	1.276(5)	C(12)–O(2) 1.263(5)	
O5–O1					2.599(3)	
O5–O3					2.599(3)	
Ru2–P3			2.252(4)	2.2584(12)		S1–C6 1.718(7)
Ru2–P4			2.236(4)	2.2313(12)		S2–C6 1.715(7)
Ru2–X5			2.081(10)	2.109(3)		N1–C6 1.329(9)
Ru2–X6			2.241(9)	2.199(3)		N1–C7 1.467(9)
Ru2–X7			2.215(11)	2.182(3)		N1–C9 1.452(5)
Ru2–X8			2.097(9)	2.139(3)		
Bond angles						
X1–Ru1–X2	60.76(12)	60.67(8)	59.6(4)	60.55(11)		71.94(6)
X3–Ru1–X4	61.17(12)	61.76(12)	59.3(3)	60.66(10)		71.94(6)
P1–Ru1–P2	99.58(5)	97.95(3)	96.53(13)	95.48(4)	98.39(4)	100.64(9)
P1–Ru1–X1	89.63(9)	88.00(7)	97.2(2)	90.58(8)	N(1)–Ru(1)–P(1) 88.29(10)	89.17(6)
P1–Ru1–X2	89.77(9)	93.05(6)	155.3(3)	93.94(8)	O(4)–Ru(1)–P(1) 96.72(9)	104.75(6)
P1–Ru1–X3	165.24(10)	168.62(9)	94.8(3)	161.76(8)	O(2)–Ru(1)–P(1) 175.07(8)	163.41(6)
P1–Ru1–X4	108.48(9)	108.18(8)	95.1(3)	102.63(8)	O(5)–Ru(1)–P(1) 89.80(8)	104.75(6)
P2–Ru1–X1	166.19(9)	107.89(6)	96.1(3)	103.91(8)	N(1)–Ru(1)–P(2) 98.24(10)	163.41(6)
P2–Ru1–X2	108.67(9)	163.95(6)	94.5(3)	161.91(8)	O(4)–Ru(1)–P(2) 89.71(10)	92.50(6)
P2–Ru1–X3	90.84(9)	88.00(8)	156.5(2)	93.62(8)	O(2)–Ru(1)–P(2) 84.78(9)	89.17(6)
P2–Ru1–X4	87.90(10)	91.50(7)	99.2(3)	95.76(8)	O(5)–Ru(1)–P(2) 171.79(8)	104.75(6)
X5–Ru2–X6			60.5(4)	61.13(11)		
X7–Ru2–X8			61.4(4)	60.70(12)		
P3–Ru2–P4			96.48(14)	96.12(4)		
X1–C11–X2	120.2(5)	118.1(3)	121.9(13)	118.3(4)	O(1)–C(12)–O(2) 126.0(4)	111.4(4)
X3–C13–X4	118.4(5)	119.2(3)	120.6(12)	118.8(4)	O(3)–C(11)–O(4) 125.8(4)	111.4(4)
X5–C17–X6			118.1(14)	118.5(4)		
X7–C19–X8			120.9(14)	117.9(4)		
X1–C11–C12	120.0(5)	119.7(3)	117.1(12)	120.5(4)		
X2–C11–C12	119.9(5)	122.2(3)	120.8(12)	121.2(4)		
X3–C13–C14	119.0(5)	117.3(4)	123.2(12)	121.5(4)		
X4–C13–C14	122.6(5)	123.5(5)	115.9(11)	119.7(4)		
X5–C17–C18			122.5(13)	120.3(4)		

Table 2 (*Continued*)

1a	**1b**	**1c**	**1c**·1.25H_2O	**2**·CH_3CN·0.5H_2O	**3**·2CH_2Cl_2·2H_2O
X6–C17–C18		119.4(13)	121.2(4)		
X7–C19–C20		123.7(13)	121.3(4)		
X8–C19–C20		115.1(13)	120.8(5)		
C11–C12–C15	114.3(3)				
C13–C14–C16	113.5(5)				
O5–H5c–O1				164	
O5–H5f–O3				164	
S1–C6–N1					122.1(6)
S2–C6–N1					126.5(5)
C7–N1–C9					117.5(6)

(For compounds **1a**, **1b**, and **1c**, X = O; For compound **3**, X = S).

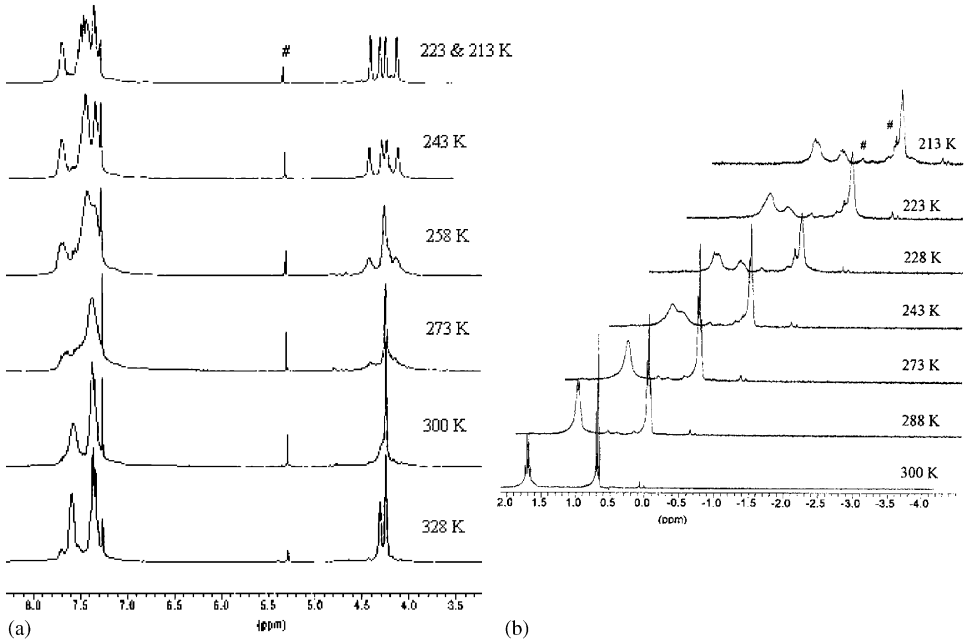

Fig. 6. VT ^{1}H-NMR spectra of (a) $Ru(RCOO)_2$dppf (R = CH_3 (**1a**), R = CH_3CH_2 (**1b**)); (b) Ethyl group proton resonances of **1b**. (#, from an impurity).

invariant P resonance in **1a** and **1b**, the P signal of **1c** exhibits VT-behaviour. The sharp signal at δ 62.9 at 328 K shifts to δ 63.1 with broadening ($v_{1/2} = 131$ Hz at 258 K), before resolving into several peaks which at 213 K are seen at (C) δ 62.9, (D) δ 63.8 and δ 65.5 (both d, $J_{PP} = 42$ Hz) and (E) δ 59.8, with relative intensities 1.5:2:1. These observations are consistent with the occurrence of a facile dynamic process at higher temperatures, equilibrating all the P atoms, e.g. a rapid monodentate–bidentate exchange of the carboxylate ligand, as reported previously for RuCl(OAc)(Cyttp) (ttp = $PhP(CH_2CH_2CH_2PPh_2)_2$) [3] and $Ru(OAc)_2PPh_3$-(dppm) (dppm = $Ph_2P(CH_2)PPh_2$) [5]; slowing down of the process with lowering of temperature, allows the "freezing out" of isomers containing monodentate and bidentate benzoate ligands shown in Fig. 9. It is here proposed that at 213 K, the P signal (C) and the corresponding proton signals at δ 4.33 ($v_{1/2} = 7$ Hz) and δ 4.53 ($v_{1/2} = 28$ Hz) be assigned to the bis(bidentate) isomer C, the P signal (D) and the proton signals at δ 4.25 and 4.22 with peak(s) overlapping with δ 4.33 to the bidentate–monodentate isomer D, and the P singlet peak (E) and the two proton singlets at δ 4.15 and δ 4.61 to the bis(monodentate) isomer E. The presence of a mixture of isomers is in agreement with the increased complexity of the multiplet for the phenyl protons at temperatures below 233 K. In view of the high reactivity expected of the coordinatively and electronically unsaturated 16e isomer $Ru(\eta^2$-PhCOO)$(\eta^1$-PhCOO)(dppf) (D′) and the 14e isomer $Ru(\eta^1$-PhCOO$)_2$(dppf) (E′), it is very likely they are present as the six-coordinate 18e solvento complexes D and E. In the presence of a good coordinating solvent, like CH_3CN, such a solvento complex (**2**) is indeed obtained (Scheme 3); herein the unbound O atoms of bis(unidentate) benzoate are hydrogen-bonded to a water ligand, which we believe

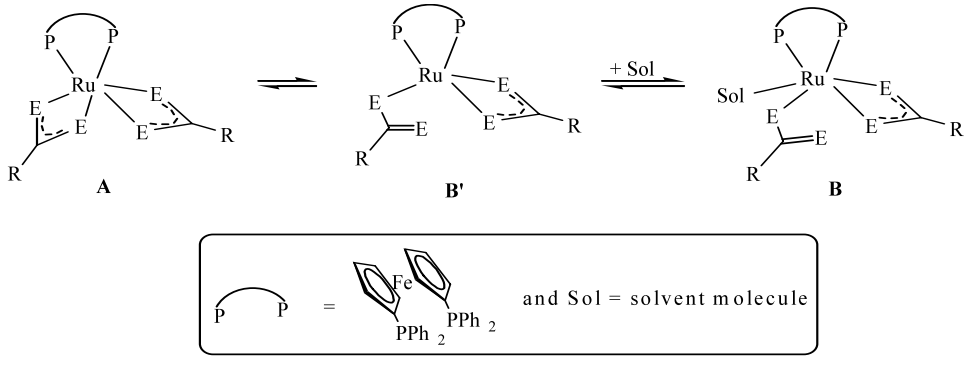

Fig. 7. Proposed isomers of **1b** and **3**. (**1b**: E = O, R = CH_2CH_3; **3**: E = S, R = $N(CH_2CH_3)_2$).

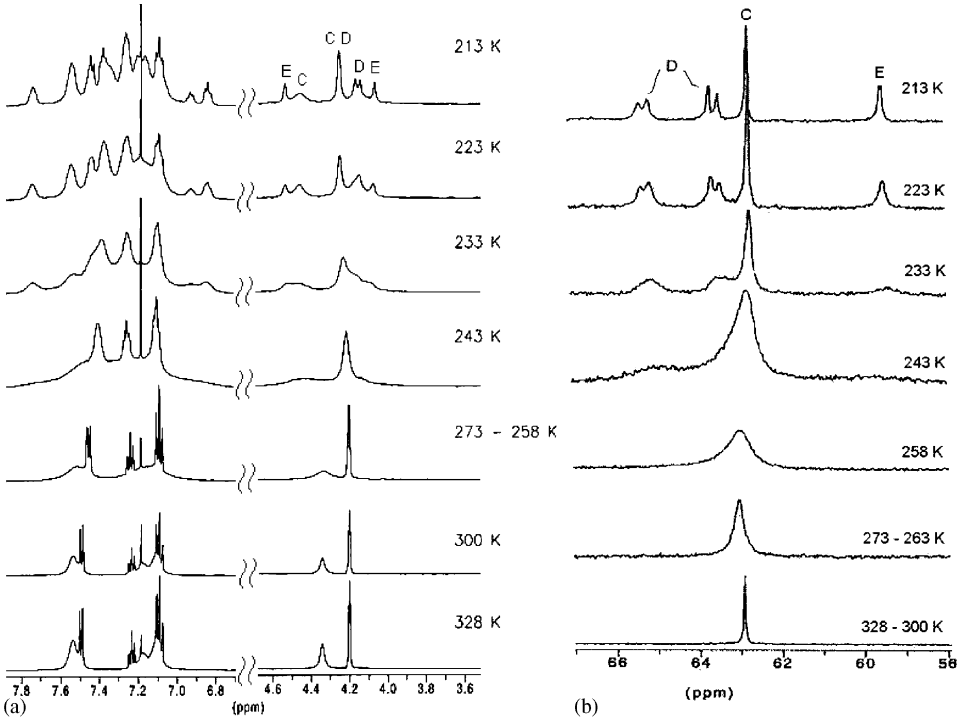

Fig. 8. VT NMR spectra of $Ru(PhCOO)_2dppf$ (**1c**) in $CDCl_3$: (a) ^1H spectra and (b) $^{31}P\{^1H\}$ spectra.

originates from water in the crystal lattice of **1c**, since the reaction was carried out in dried solvent. The non-isolation of a monodentate carboxylate of **1a** is consistent with no indication of uni- and bidentate exchange in studies of its VT-NMR spectral behaviour. However, though this exchange is observed in the VT-NMR spectra of **1b**, a monodentate carboxylate derivative from **1b** has not been isolated. Presumably, the facile bidentate–unidentate transformation in **1c** is facilitated by the electron-withdrawing effect of the phenyl ring in weakening the M-O(carboxylate) bond.

The VT proton spectral changes of **3** in $CDCl_3$ are shown in Fig. 10. At 328 K, the proton spectrum of complex **3** shows one sharp unresolved triplet at δ 1.00 for the two Me groups and broad signals with relative intensity ca. 1:3 at δ 3.33 ($v_{1/2} = 46$ Hz) and 3.62 ($v_{1/2} = 29$ Hz) for the CH_2 protons, and four equal-intensity singlets at δ 4.19, 4.32, 4.42 and 4.45 for the Cp protons of dppf. The phenyl protons are seen as a singlet at δ 7.70 together with a multiplet at δ 7.24–7.19 (relative intensity 2:3). As the temperature is lowered, the multiplicity of the Cp resonances changes, indicative of alteration in equivalence of the rings. The ^{31}P signal of

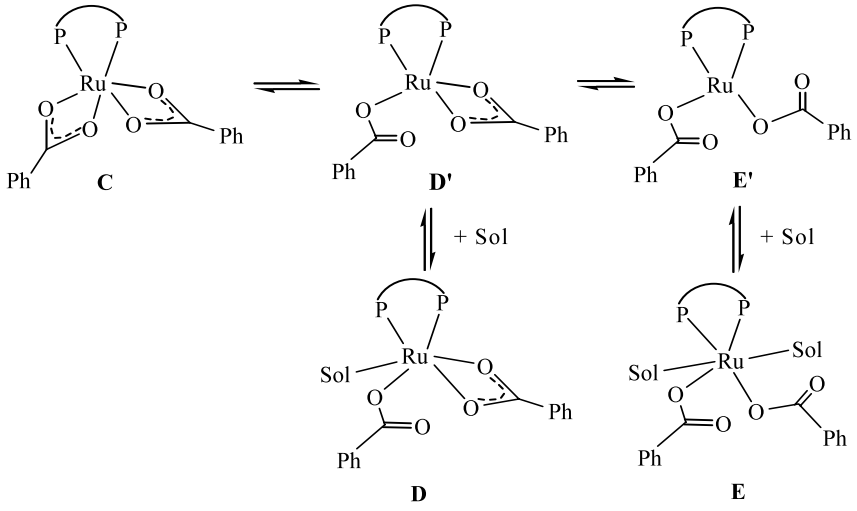

Fig. 9. Proposed isomers of [$Ru(PhCOO)_2dppf$] (**1c**).

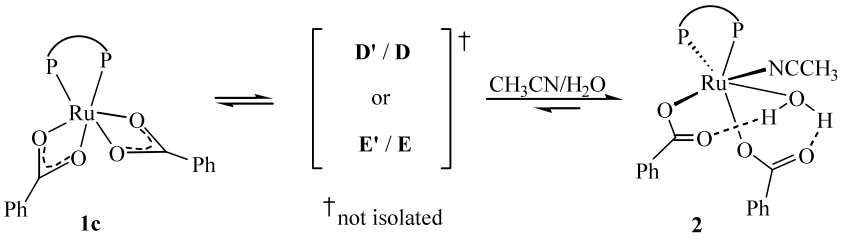

Scheme 3.

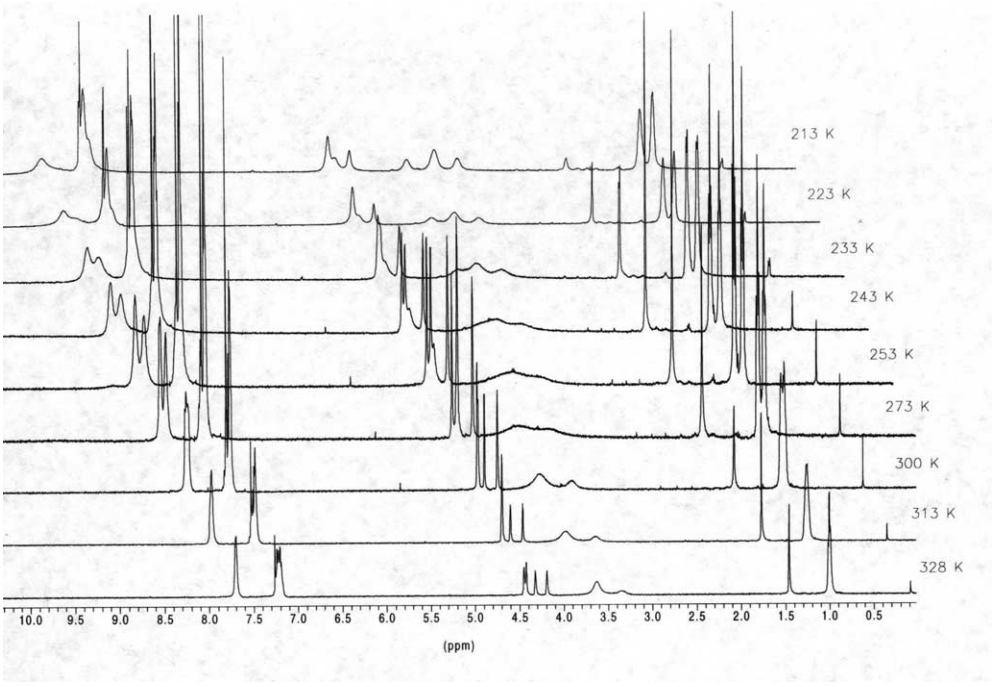

Fig. 10. VT ^{1}H-NMR spectra of Ru(SC(S)NEt$_2$)$_2$(dppf) (**3**) in $CDCl_3$.

the dithiocarbamate complex **3** remains essentially temperature-invariant, with only a small variation in the chemical shift and line-width of the singlet signal as follows: 328 K, δ 47.1 ($\nu_{1/2} = 86$ Hz); 300 K, δ 48.9 ($\nu_{1/2} = 110$ Hz); 273 K, δ 48.8 ($\nu_{1/2} = 336$ Hz); 243 K, δ 48.5 ($\nu_{1/2} = 259$ Hz); 233 K, δ 48.6 ($\nu_{1/2} = 173$ Hz); 223 K, δ 48.9 ($\nu_{1/2} = 81$ Hz); 213 K, δ 49.1 ($\nu_{1/2} = 48$ Hz), indicating rapid exchange processes. The variation in line broadening is in agreement with similar variations in the methylene resonances of the ethyl group, discussed below. With decrease of temperature, the Me resonance becomes resolved into two triplet signals of equal intensity, becoming fully resolved at 253 K (δ 0.98 and 0.88), in agreement with inequivalent Me groups. This suggests that at these low temperatures, the molecule is totally in the form of species B′/B (Fig. 7), with one monodentate dithiocarbamate ligand, since more than two Me resonances are expected for a mixture of isomer A and B′/B or only one resonance for isomer A. Below 300 K, the CH_2 resonances broaden, merging at 253 K into a broad "band" centred at δ 3.47 ($\nu_{1/2} = 185$ Hz), before emerging again as three broad peaks, which at 213 K are observed at δ 3.00, 3.26 and 3.58 ($\nu_{1/2}$ ca. 23 Hz) (relative intensity 1:2:1). The incidence of uni- and bidentate dithio ligand exchange as suggested here is reminiscent of earlier examples, viz. $(C_5Me_5)M(S_2CNMe_2)_2$ (M = Rh, Ir), conclusively studied via kinetic line-shape analysis [30] and $CpMo(NO)(S_2COMe)_2$, also studied by VT-NMR spectral analysis [31]. Indeed, such phenomena are quite common in transition metal complexes containing (S–S) ligands and it has been pointed out in previous reports that simultaneous mono- and bidentate coordination of the S–S groups may arise because of geometrical constraints imposed by the central metal atom or electronic factors [32,33]. There is no evidence of monomer–dimer equilibrium in **3** as found for $[Os(S_2CNEt_2)_3]^+$ [34].

4. Conclusion

The bis($RCOO^-$) and bis($S_2CNEt_2^-$) ligands of Ru(dppf) complexes exhibit temperature-dependent

uni-bidentate exchange for R = Et and Ph, but not for R = Me. This fluxional difference among the analogues was not expected. VT-NMR spectral observations of the acetate and propionate complexes are consistent with fluxionality of the bidentate dppf ligand involving concerted twisting of the Cp rings around its axis and bridge-reversal at Ru. These ligand geometric and coordination mobilities, together with the stereochemical non-rigidity of the metal would make these complexes potentially catalytic. The catalytic role of similar carboxylate complexes in Pd(II) in Heck-type syntheses is well documented. Our immediate target is to examine related behaviour of these Ru(II) complexes and their potential as precursors to enter into mixed-metal carboxylates.

5. Supplementary material

Crystallographic data for the structural analyses have been deposited with the Cambridge Crystallographic Data Centre; **1a**: CCDC No. 202630; **1b**: 202631; **1c**: 202632; **1c**·1.25H_2O: 202633; **2**·CH_3CN·0.5H_2O: 202634 and **3**·2CH_2Cl_2·2H_2O: 202635. Copies of this information may be obtained free of charge from The Director, CCDC, 12 Union Road, Cambridge CB12 1EZ, UK (Fax: +44-1223-336033; e-mail: deposit@ccdc.cam.ac.uk or www: http://www.ccdc.cam.ac.uk).

Acknowledgements

Support of the National University of Singapore in the form of Grant Nos. RP14300077112 and RP143000135112 to L.Y.G. and research scholarship to X.L.L. is gratefully acknowledged.

References

[1] S.J. Sherlock, M. Cowie, Organometallics 7 (1988) 1663.
[2] R.W. Hilts, S.J. Sherlock, M. Cowie, E. Singleton, M.M.de.V. Steyn, Inorg. Chem. 29 (1990) 3161.
[3] G. Jia, A. Rheingold, B.S. Haggerty, D.W. Meek, Inorg. Chem. 31 (1992) 900.
[4] E.B. Boyar, P.A. Harding, S.D. Robinson, J. Chem. Soc. Dalton Trans. (1986) 1771.
[5] W.-K. Wong, K.-K. Lai, M.-S. Tse, M.-Ch. Tse, J.-X. Gao, W.-T. Wong, S. Chan, Polyhedron 13 (1994) 2751.
[6] P. Sengupta, S. Ghosh, T.C.W. Mak, Polyhedron 20 (2001) 975.
[7] A.D. Zotto, E. Rocchini, F. Pichierri, E. Zangrando, P. Rigo, Inorg. Chim. Acta 299 (2000) 180.
[8] L. Matas, J. Muniente, J. Ros, A. Alvarez-Larena, J.F. Piniella, Inorg. Chem. Commun. 2 (1999) 364.
[9] R.W. Mitchell, A. Spencer, G. Wilkinson, J. Chem. Soc. Dalton Trans. (1973) 846.
[10] A. Begiun, H.-C.h. Bottcher, G. Suss-Fink, B. Walther, J. Chem. Soc. Dalton Trans. (1992) 2133.
[11] A. Salvini, P. Frediani, F. Piacenti, J. Mol. Catal. A: Chem. 159 (2000) 185.
[12] R. Noyori, Chem. Soc. Rev. 18 (1989) 187 (and references therein).
[13] B. Heiser, E.A. Broger, Y. Crameri, Tetrahedron: Asymmetry 2 (1991) 51.
[14] J.P. Genet, S. Mallart, C. Pinel, S. Juge, J.A. Laffitte, Tetrahedron: Asymmetry 2 (1991) 43.
[15] N.W. Alcock, J.M. Brown, M. Rose, A. Wienand, Tetrahedron: Asymmetry 2 (1991) 47.
[16] H. Doucet, P.L. Gendre, C. Bruneau, P.H. Dixneuf, J.-C. Souvie, Tetrahedron: Asymmetry 7 (1996) 525.
[17] K.S. Gan, T.S.A. Hor, in: A. Togni, T. Hayashi (Eds.), Ferrocenes, Homogeneous Catalysis, Organic Synthesis and Materials Science, VCH Weinheim, 1995 (Chapter 1 and references therein)
[18] T. Ishiyama, M. Mori, A. Suzuki, N. Miyaura, J. Organomet. Chem. 525 (1996) 225.
[19] J. Louie, M.S. Driver, B.C. Hamann, J.F. Hartwig, J. Org. Chem. 62 (1997) 1268.
[20] B.H. Simmons, Inorg. Synth. 12 (1970) 238.
[21] J.D. Gilbert, G. Wilkinson, J. Chem. Soc. (A) (1969) 1749.
[22] M. Menon, A. Pramanik, N. Bag, A. Charkravorty, J. Chem. Soc., Dalton Trans. 10 (1995) 1543.
[23] SMART and SAINT Software Reference manuals, version 6.22, Bruker AXS Inc., Madison, WI, 2000.
[24] G.M. Sheldrick, SADABS software for empirical absorption correction, University of Göttingen, Göttingen, Germany, 2000.
[25] SHELXTL Reference Manual, version 5.1, Bruker AXS Inc., Madison, WI, 1998.
[26] G. Suss-Fink, G. Herrmann, P. Morys, J. Ellermann, A. Veit, J. Organomet. Chem. 284 (1985) 263.
[27] (a) G.B. Deacon, R.J. Phillips, Coord. Chem. Rev. 33 (1980) 227; (b) K. Nakamoto, Infrared and Raman Spectra of Inorganic and Coordination Compounds, 5th ed, Wiley, New York, 1997, p. 232.
[28] (a) L.H. Pignolet, S.H. Wheeler, Inorg. Chem. 19 (1980) 935; (b) A. Elduque, C. Finestra, J.A. López, F.J. Lahoz, F. Merchán, L.A. Oro, M.T. Pinillos, Inorg. Chem. 37 (1998) 824; (c) P.J. Heard, K. Kite, J.S. Nielsen, D.A. Tocher, J. Chem. Soc. Dalton Trans. (2000) 1349.
[29] L. Pauling, The Nature of the Chemical Bond, 3rd ed, Cornell University Press, Ithaca, NY, 1960, pp. 224–229.
[30] R. Robertson, T.A. Stephenson, J. Chem. Soc. Dalton Trans. (1978) 486.
[31] W. De Oliveira, J.-L. Migot, M.B. De, L.J. Sala-Pala, J.-E. Guerchais, J.-Y. Le Gall, J. Organomet. Chem. 284 (1985) 313.
[32] D.F. Steele, T.A. Stephenson, J. Chem. Soc. Dalton Trans. (1973) 2124.
[33] M.C. Cornock, R.O. Gould, C.L. Jones, J.D. Owen, D.F. Steele, T.A. Stephenson, J. Chem. Soc. Dalton Trans. (1977) 496.
[34] S.H. Wheeler, L.H. Pignolet, Inorg. Chem. 19 (1980) 972.